A&A 381, 683–693 (2002)
DOI: 10.1051/0004-6361:20011513

Astronomy & Astrophysics

The dynamics of an erupting prominence

K.-L. Klein and Z. Mouradian

Observatoire de Paris, Section de Meudon, DASOP & CNRS-UMR 8645, 92195 Meudon, France
e-mail: zadig.mouradian@obspm.fr

Received 11 May 2001 / Accepted 19 October 2001

Abstract. Hα full disk observations and radio interferometry at decimetre and metre wavelengths are used to probe the dynamics of ejecta and electron acceleration during a solar eruptive event on 1990 September 14. An erupting prominence and a moving type IV radio source are shown to trace a common magnetic structure during its rise from ∼10 Mm to 3 $R_\odot$ above the limb. The height-time plot excludes a purely ballistic flight in the height range (0.5–3) $R_\odot$, but is consistent with both constant acceleration and constant velocity at heights $\geq$0.5 $R_\odot$. A plasma model of the radio emission is used to infer the mass and energetics of the ejected material. Electrons are accelerated in the surroundings of the rising structure, and in two flares up to 70° away from the prominence. Radio observations provide evidence for large-scale interconnecting loops, but a physical connection between the eruption and the remote flares cannot be demonstrated.

Key words. Sun: activity – corona – CMEs – filaments – flares – radio radiation

1. Introduction

Erupting prominences (*disparitions brusques*) and moving type IV metre wave radio sources reveal the destabilisation of magnetic structures and their propagation through the low and middle corona. Both the thermal insulation, which keeps part of the prominence material neutral so that it is visible in Hα, and the confinement of electrons which emit the radio waves, require magnetic fields and make the respective emissions a tracer of the dynamics of ejected magnetic field structures. Hα and radio observations therefore enable one to study the dynamics of more localised and better defined configurations within a coronal mass ejection (CME) than its white-light signature, where it is especially difficult to separate the bulk motion of the plasma from its expansion. Hα and radio observations have the further advantage of tracing both emission above the limb and on the disk and to allow studies of CME-associated activity. A review on prominence eruptions is given by Démoulin & Vial (1992).

Moving type IV bursts are observed at metre and decametre wavelengths. They are emitted by suprathermal electrons through either the gyrosynchrotron process (Dulk 1973) or plasma emission (Robinson 1978; Duncan 1981; Trottet et al. 1981). The radio sources are characterised by systematic outward motions over distances up to several solar radii, and are often associated with prominence eruptions (cf. Robinson 1978; Stewart 1985). A review of moving type IV bursts is given by Stewart (1985), and the relationship with prominences is extensively discussed in MacQueen (1980, and references therein) (cf. Stewart et al. 1982; Kurokawa et al. 1987; Gopalswamy & Kundu 1989, for more recent work). From these analyses it appears that Hα and metre wave radio observations trace substructures of a CME and are able to provide valuable information on the dynamics of the ejecta.

On 1990 September 14 the eruption of a prominence which could be tracked to unusual heights for ground-based whole Sun observations, and an unusually long lasting moving type IV radio source were observed above the eastern solar limb together with flares in several active regions in the eastern hemisphere. We present (Sect. 2) the coronal context of the event (Sect. 2.1), the Hα and radio observations (Sect. 2.2) during the eruptive event and an overview on simultaneous activity on the disk (Sect. 2.3). The observations are summarised in Sect. 2.4. In Sect. 3 we interpret the structure (Sect. 3.1) and dynamics of the ejecta (Sect. 3.2), derive an estimate of mass and energetics from a plasma emission model of the type IV burst (Sect. 3.3), and discuss qualitatively scenarii of electron acceleration associated with the eruption (Sect. 3.4).

2. Observations

The Hα line observations were performed with the 3-λ Heliograph in Meudon. The bandwidth of the filter (Demarcq et al. 1985) is 0.5 Å. The instrument takes one image of the Sun in the centre of the Hα line and two

Send offprint requests to: K.-L. Klein,
e-mail: ludwig.klein@obspm.fr

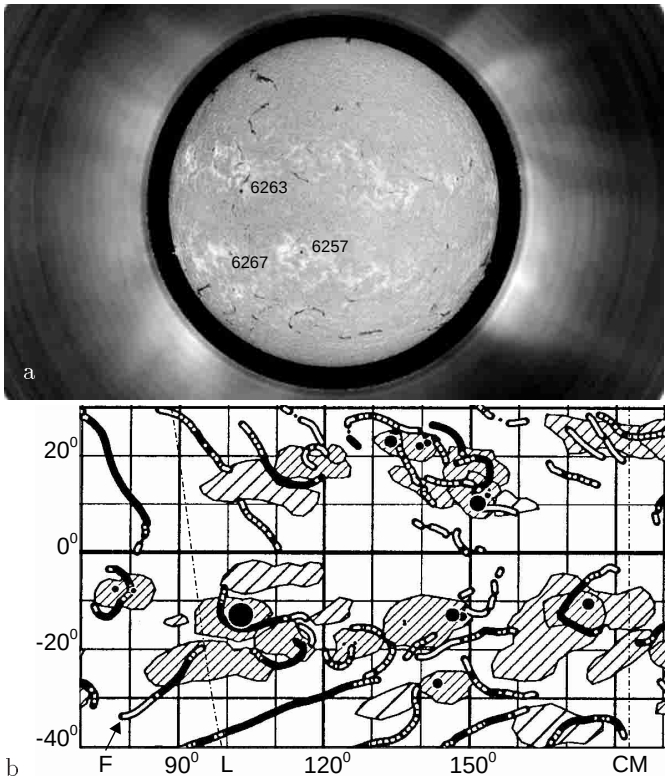

Fig. 1. Active regions and coronal structures prior to the eruptive event on 1990 September 14: **a)** Meudon Hα spectroheliogram (1990 Sep. 14, 07:06 UT) and Mauna Loa K-coronameter image (1990 Sep. 13, 17:39 UT). North is at the top, west to the right. Relevant active regions are marked by their NOAA numbers (*Solar Geophysical Data*). **b)** Synoptic map of filaments and active regions during Carrington rotation 1833 (Meudon Observatory). Dashed-dotted lines show the eastern solar limb (marked L below the abscissa) and the central meridian (marked CM) at 13:30 UT on September 14. The filament which undergoes the *disparition brusque* is marked F in the lower left corner of the map.

in the wings ($\pm$0.5 Å). For the study of prominences one overexposed image is taken in the line centre every 10 min. On 1990 September 14 one set of images was taken every 1.5 min from 06:47 to 16:07 UT.

Radio maps were provided by the Nançay Radioheliograph (NRH; Radioheliograph Group 1989). In 1990 each of its two orthogonal interferometer arrays measured one-dimensional brightness distributions of the corona: the north-south array at five frequencies (in the event studied: 164, 237, 327, 408, 435 MHz, corresponding to wavelengths of 1.83, 1.27, 0.92, 0.73, 0.69 m), and the east-west array at 164 MHz. This provides the localisation of the centroid and the dimension of the source projected onto the interferometer baselines, i.e. determination of the complete plane-of-the-sky position at 164 MHz, but of only one coordinate at higher frequencies. Spectral identification of the emissions was provided by the spectrographs of the Astrophysical Institute Potsdam in Tremsdorf (H. Aurass) and of the Space Research Dept. of Paris Observatory in Nançay (M. Poquérusse).

2.1. Prolog: Pre-eruptive structures in the eastern hemisphere on 1990 September 14

The prominence eruption occurred near 13 UT on the south-eastern limb. Structures of the corona and active regions are presented in Fig. 1.

In the pre-event Hα spectroheliogram (Fig. 1a) the prominence is seen above the limb east of active region NOAA 6267. Judging from the synoptic map of filaments and active regions during Carrington rotation 1833 (Mouradian & Zlicaric 1998, Fig. 1b), the prominence is the north-western end of a filament that lay at and beyond the limb, in an old plage at Carrington longitude $L = 88°$, latitude $\phi = -28°$ (marked F in the lower left corner of Fig. 1b). The active region was decaying from a very complex configuration in the preceding rotation. A pivot point was located at the north-western end of the prominence ($\phi = -19.5°$, $L = 93°$). Such pivot points (Mouradian et al. 1987) are regions where magnetic flux emerges, and are frequently associated with the disconnection of magnetic field structures during the dynamic disappearance of filaments (e.g. Mouradian et al. 1998). The filament in Fig. 1b is actually the one which reformed after the eruption. It became first visible on September 16. The newly formed filament usually has the same shape as the one that disappeared.

2.2. The prominence eruption and moving type IV radio burst

Comparison of the white-light corona before (Fig. 1a) and after the eruptive event (Fig. 4d) shows that material was blown out above the site of the filament between 17:39 on September 13 and 17:47 on September 14. Although we have no simultaneous coronographic observations, we therefore conclude that the eruptive event under discussion was part of a coronal mass ejection (CME).

2.2.1. Hα observations

The time history of the prominence eruption is shown by the sequence of line centre images of Fig. 2. The first signature of the prominence liftoff was observed at 12:56 UT, when its height started to increase. Subsequently the north-western leg became more dilute (e.g. 13:15:45) and eventually invisible (13:29:13), whereas, as usual (Mouradian et al. 1995), the other footpoint remained anchored until the end of the eruption process. From the latitude of the stable leg seen above the limb and the synoptic map in Fig. 1, this footpoint is probably rooted at $\phi \simeq -26°$, $L \simeq 90°$. During its initial rise (until 13:30 UT) the prominence was seen to untwist, as in other events (cf. Kurokawa et al. 1987; House & Berger 1987; Vršnak et al. 1993; Plunkett et al. 2000). Between 13:35 and 13:46 UT a bright blob detached from the leading edge of the rising prominence. The snapshot at 13:35:28 UT shows the still connected south-eastern leg of the prominence, on top of it the partially detached blob, and below a bright surge

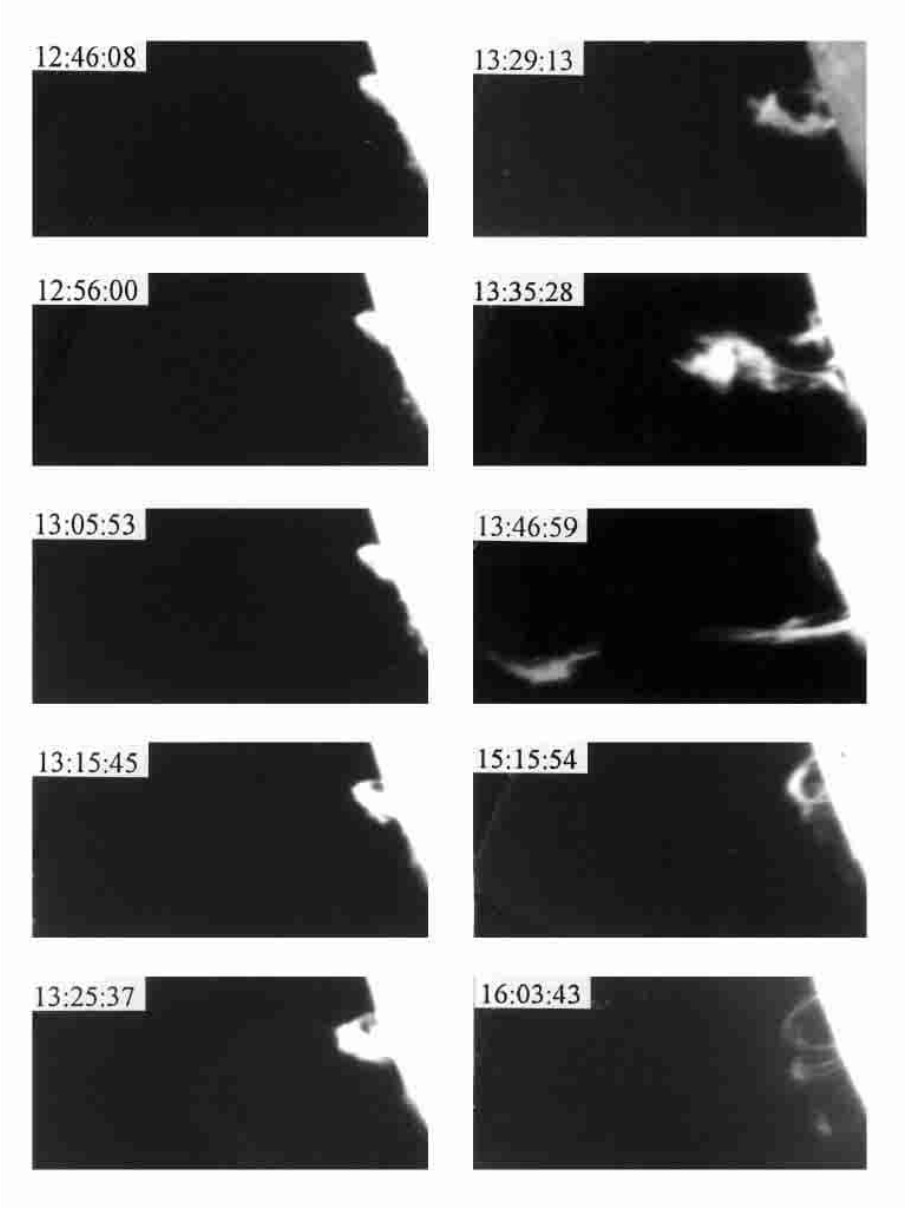

Fig. 2. The erupting prominence (12:46:08–13:46:59), surge (13:35:28) and flare loop system (13:46:59–16:03:43) above the eastern solar limb on 1990 September 14 (3λ Heliograph, Meudon). Solar north is at the top, east to the left.

at the place where the north-western leg was rooted before the eruption. Since surges usually occur at sites with a parasitic magnetic polarity, this gives further evidence that the disconnected leg of the prominence was previously anchored at a site of magnetic flux emergence, where magnetic reconnection likely occurs (Mouradian et al. 1998). The snapshot at 13:46:59 UT shows the prominence near the time of its largest extent in Hα. Its body has straightened, and the detached blob is rising ahead of it, while other material seems to fall back to the Sun. This may reveal either the actual downflow of cool material or its heating and ionisation, which make an increasing part of the prominence body invisible in Hα. The prominence and blob faded from view in Hα near 13:50 UT, when the blob had reached an altitude of 0.5 $R_\odot$ above the photosphere.

A system of arches with summits at increasing height was observed underneath the rising prominence since 13:42 UT (Fig. 2). The alignment of multiple arches in the last image in Fig. 2 suggests that they formed an arcade bridging the location of the former prominence. Following work on eruptive events on the disk (cf. McAllister et al. 1992; Hanaoka et al.1994; van Driel-Gesztelyi et al. 1997; Khan et al. 1998; Mouradian et al. 1998; Czaykowska et al. 1999), we identify these arches with the flare loops that form below the ejected structure and connect the flare ribbons which are expected to lie behind the limb in the present event. At the end of our Hα observations the loop tops were at a height of 45 000 km and still slowly rising.

The height-time trajectories of the highest points of the prominence, surge and flare loops are plotted in Fig. 3. The tops of the flare loops rose at an apparent speed that gradually decreased from 20 to 2 km s^{-1}. The prominence trajectory is plotted by open triangles. The curved line represents a quadratic least squares fit to the measurements after 13:10 UT. Usually the liftoff of a prominence proceeds in two phases, consisting of a slow rise due to the

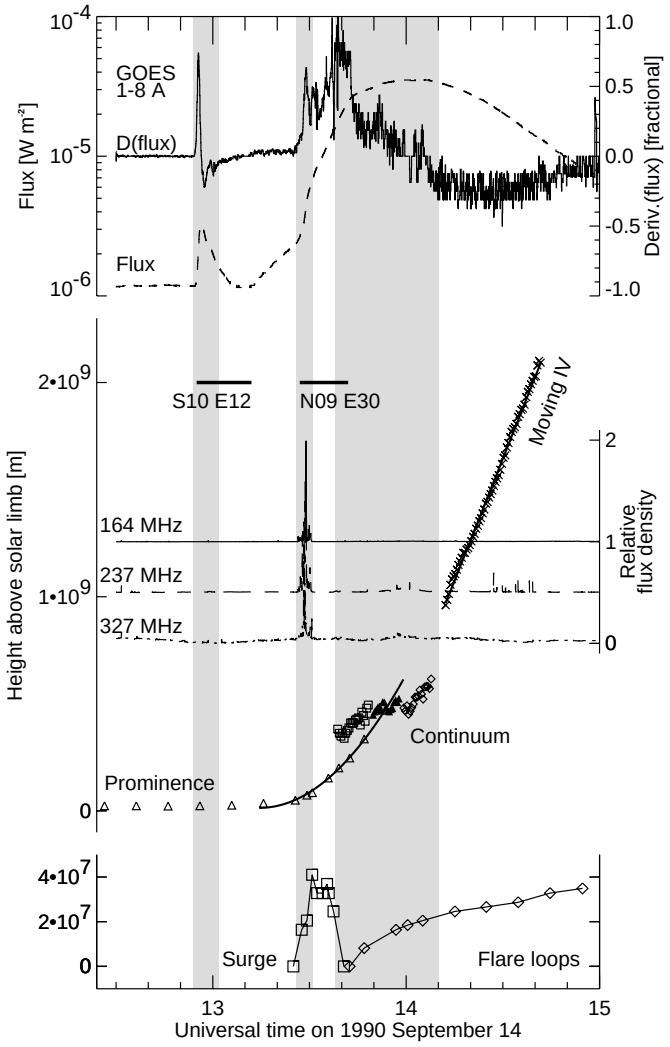

Fig. 3. Height-time plots and radiative time histories during the event. Vertical grey stripes highlight different episodes of radio emission: impulsive centimetre wave burst (12:54–13:02 UT), metric type III/V bursts (13:26–13:31 UT), metric continuum emission (13:37–14:10 UT). The lower half of the figure displays the height-time diagrams of the tips of the surge (open squares), flare loops (diamonds) and the erupting prominence (triangles), and of the centroids of radio sources at 164 MHz (continuum: open squares, filled triangles, open diamonds as in Fig. 4; moving type IV source: ×). The whole Sun metric radio emission in the centre of the panel is dominated by type III/V bursts. The soft X-ray flux (dashed line) and its time derivative (solid line labelled "D(flux)") are plotted in the upper half, together with time intervals and locations of Hα flares (after *Solar Geophys. Data*).

straightening of the arch-shape and a subsequent ejection of the plasma and magnetic field into the corona. We surmise from other observations (Mouradian et al. 1995) that the pronounced accelerated rise after 13:10 UT was actually the second phase of the prominence ascent, and that the early phase was only partly visible in our data, because the body of the prominence lay behind the limb. A number of height-time trajectories of disappearing filaments is shown in Fig. 50 of Rompolt (1990).

2.2.2. Moving type IV radio source

Radio sources observed during and after the rise of the prominence are overlaid in Fig. 4 on about time-coincident Hα images. We defer discussion of the events on the disk (Figs. 4a,b) to Sect. 2.3. A moving radio source was observed between about 14:13 and 14:40 UT at 164 MHz (Fig. 4c).

Trajectory of the radio source

The centroid position and size of a radio source were identified as the position of the maximum and the half-width of a Gaussian fitted to the one-dimensional scans of the NRH. Scans integrated over 30 s were used, from which an average post-event image (14:40–14:50 UT) had been subtracted. The trajectory and size of the source at 164 MHz are plotted as connected crosses in Fig. 4c. The source emerged out of a complex of stationary and moving sources whose centroids are plotted by various symbols above the erupting prominence (cf. Sect. 2.2.3). The moving type IV source first moved eastward (14:13–14:24 UT), and then turned south-eastward (14:24–14:40 UT). Comparison with the post-eruptive corona (Fig. 4d) shows that material was evacuated above the erupting prominence and in the region where the radio emission occurred.

The height of the moving type IV source centroid as a function of time is plotted by crosses (×) in Fig. 3. The directional change of the source motion is not visible in this plot, because the north-south coordinate, where this change is conspicuous, only gives a minor contribution to the source height. The straight line through the measured points corresponds to a projected radial speed $\sim$630 km s^{-1}.

Spatial structure of the radio source

The time evolution of the source configuration is displayed in Figs. 5a–c at four frequencies of the NRH north-south branch. In each panel the images are represented as grey scales of equal 1D-brightness at 237 MHz, and overlayed as a contour plot at a different frequency. The vertical axis gives the distance from disk centre, which is the zero of the axis in each plot, measured towards terrestrial south.

The moving radio source is the feature marked "M" in Fig. 5a. The centroid positions at 164 MHz and 237 MHz are indistinguishable with the available data. Figure 5d shows this in heliographic coordinates for three positions measured at 5.5 min intervals. Although emission from the moving radio source is close to the noise level at and above 327 MHz, Figs. 5b and c suggest that a faint trace of the moving source existed at the same north-south coordinate as at 237 and 164 MHz. The emission faded the earlier, the higher the frequency. Extrapolation of the trajectory at 435 MHz (the frequency that provides the best spatial resolution with the north-south array) suggests that the moving source could be distinguished between 13:45 and 13:50 UT. But only at 164 and 237 MHz was the signal intense enough for a detailed study.

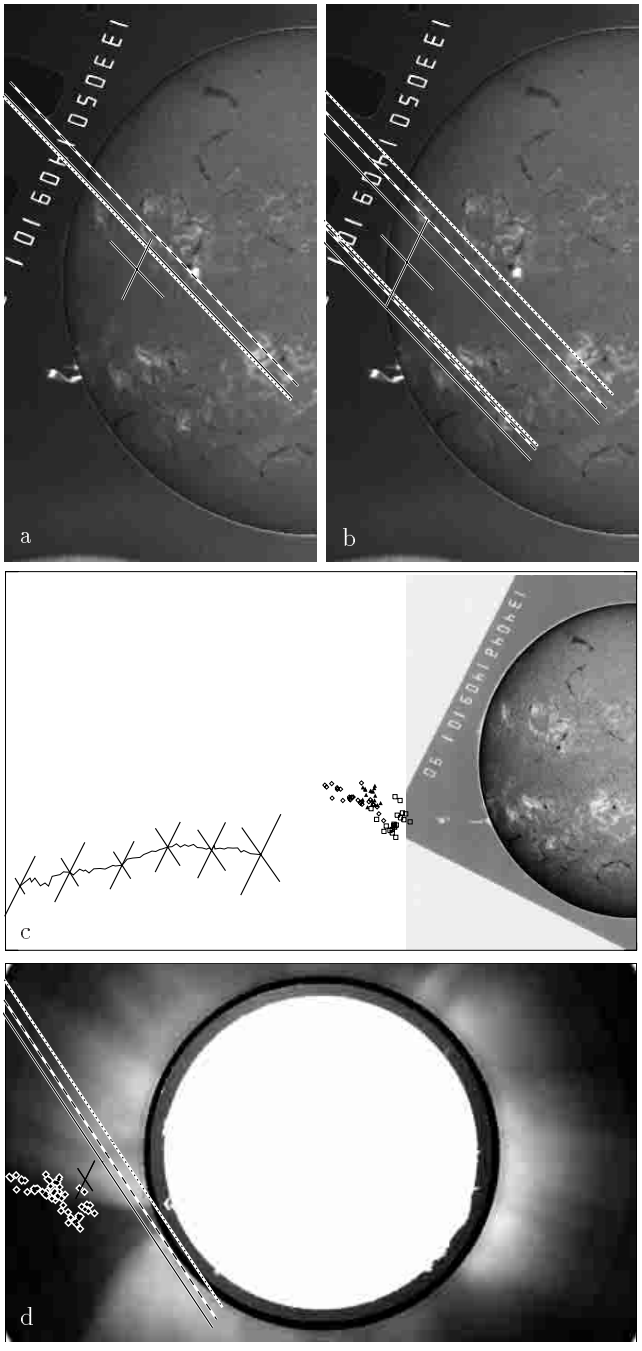

Fig. 4. Radio source positions (crosses, lines) and visible light images during the eruptive event. From top to bottom: Hα 13:30:50 UT, showing the flare in AR 6263 and the rising prominence above the eastern limb. Emission from above the limb has been artificially enhanced. **a)** Type III burst (13:28:09 UT), **b)** type V continuum (13:28:55 UT). Cross: centroid and half widths at 164 MHz; sources at higher frequencies lie on the solid (237 MHz), dashed (327 MHz) and dotted (435 MHz) lines. **c)** Hα at 13:40 UT, 164 MHz continuum sources 13:37–14:10 UT (squares, diamonds, triangles), centroids of a moving type IV source at 164 MHz (14:13–14:41 UT; continuous line), with dimensions at selected times (crosses). **d)** Hα (15:15:50 UT), Mauna Loa K-coronameter image (17:47 UT), radio source positions (∼14:20 UT) during a stationary type IV burst. The continuum positions at 164 MHz from **c)** are overplotted for comparison.

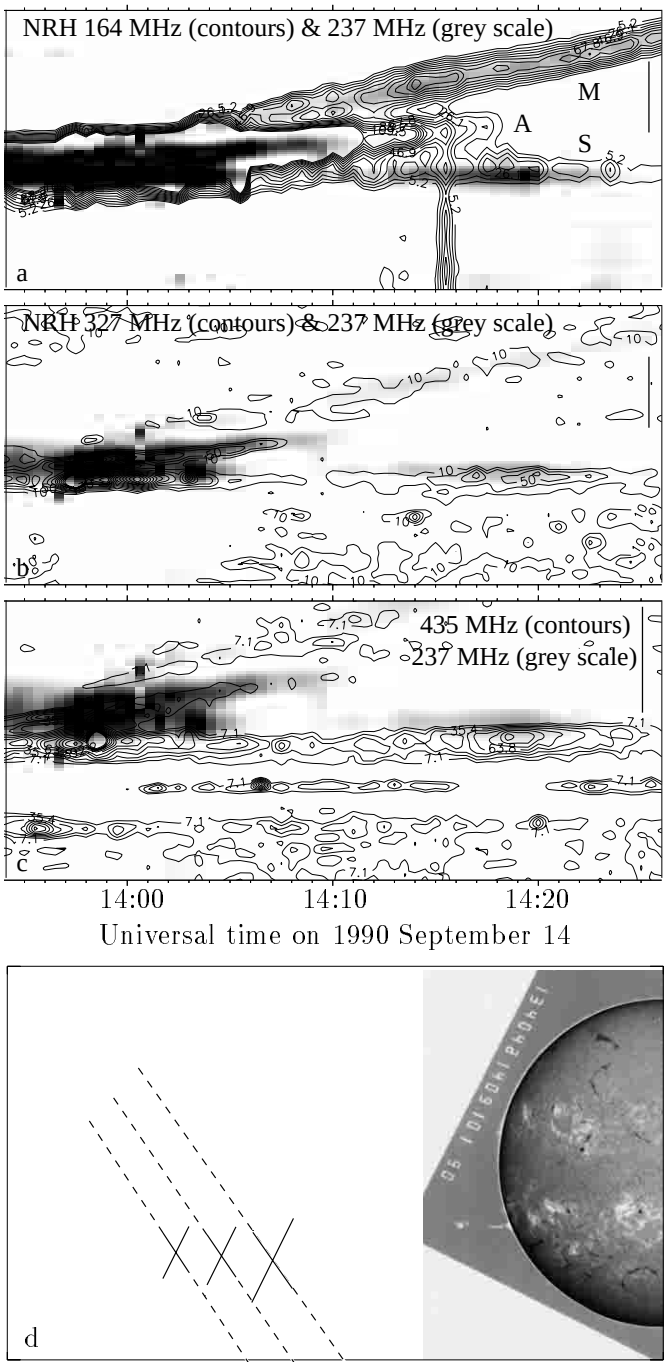

Fig. 5. Temporal evolution of the position and structure of radio sources above the south-eastern limb: **a)**–**c)** Contours of 1D brightness at three frequencies superposed on the grey-scale representation at 237 MHz. Ordinate: distance from disk centre (bottom) towards terrestrial south, over 3.8 $R_\odot$ **a)**, **b)** and 2.8 $R_\odot$ **c)**, respectively. The vertical bar near the right border has length 1 $R_\odot$. The darkest shading and highest contour correspond to 20% **a)** and 50% **b)**, **c)** of the brightness maximum within the plotted field, respectively. In **a)** "M" refers to the moving type IV source, "S" to a stationary type IV, and "A" to another moving source within a complex continuum. **d)** Hα image at 13:40 UT, moving type IV positions at 237 MHz (dashed lines) and 164 MHz (crosses) at 14:13:15, 14:18:45 and 14:24:15 UT (from right to left).

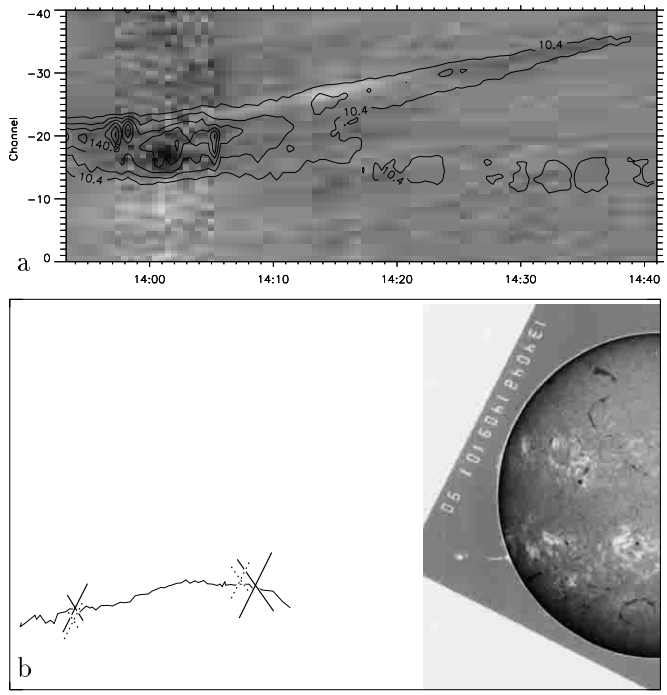

Fig. 6. a) Evolution of the 1D brightness distribution in circular polarisation (Stokes parameter V; grey scale, negative levels in white) and total brightness (contours) at 164 MHz. Vertical axis in instrument units from the disk centre (bottom) along the terrestrial east. **b)** Positions and half widths of the sources in total intensity (solid crosses) and circularly polarised intensity (dashed crosses) at 14:13:45 UT (right) and 14:35:15 UT, respectively.

The source at 164 and 237 MHz was most of the time much broader than the beam of the NRH. In the north-south scans the source was larger at 164 MHz than at 237 MHz (by ∼50%). The high-frequency source appeared to be surrounded by the low-frequency source while both rose in the corona. The source size decreased during the event at 164 MHz, especially along the terrestrial east-west direction, as illustrated by the size of the crosses in Fig. 4c (2.4×10^5 km to 9.4×10^4 km in 25 min). The decrease was slower in the north-south direction at 164 MHz (from 2.9×10^5 km to 2.2×10^5 km in 25 min), and unmeasurable at 237 MHz (1.8×10^5 km). Besides the general trend of decrease of the east-west dimension, fluctuations of the source size were observed, which point to some unresolved structure.

Circular polarisation and brightness temperature

A contour plot of total brightness of the 164 MHz emission is overlaid on a grey scale representation of circularly polarised brightness in Fig. 6a. The white shading between ∼14:10 and 14:22 UT shows right-handed circular polarisation of about 15%. The polarised source is located in the north-eastern (i.e., leading) part of the moving radio source (rightmost dashed cross in Fig. 6b). No significant polarisation was seen in the trailing part. The 237 MHz emission was also right-hand polarised until it faded from view near 14:25 UT. The 164 MHz emission persisted, but its polarisation changed to zero between 14:22 and 14:26 UT and eventually to left-handed (dark shading in Fig. 6a) until the source became invisible. During this late phase the whole 164 MHz source was polarised, as illustrated by the dashed cross in the lower left corner of Fig. 6b. The average degree of left-handed polarisation was 35%. The change of polarisation and the change of trajectory at 164 MHz occurred within a few minutes, together with the fading of the emission at 237 MHz. The configuration of Fig. 6b suggests two distinct sources which are only partly resolved in total intensity maps outline different parts of a rising structure, i.e. a north-eastern right-hand polarised component that dominated initially, but faded earlier than the south-western left-hand polarised component (cf. Sect. 3.1).

At 164 and 237 MHz the moving radio source is sufficiently well defined in individual scans that the brightness temperature can be determined. Since only one-dimensional measurements are available at 237 MHz, we suppose that the source has circular cross section. The brightness temperatures at the three instants plotted in Fig. 5d are in the range (10–13) $\times 10^6$ K at 164 MHz, and (4.2–6.1) $\times 10^6$ K at 237 MHz.

2.2.3. Radio emission around and below the rising prominence

As seen in Fig. 5, the moving type IV source emerged from a complex set of sources of broadband (continuum) emission which dominated during the time interval marked by the rightmost grey stripe in Fig. 3. The emission is hardly visible in the whole Sun flux. This period corresponds to the early stages of the flare loop formation in the low corona, to the early and most intense phase of a "gradual rise and fall" at microwave frequencies, type II radio emission from a coronal shock below 90 MHz (Tremsdorf Observatory of the Potsdam Astrophysical Institute; H. Aurass, pers. comm.), and to continued energy release as traced by the time derivative of the soft X-ray flux in Fig. 3.

The 164 MHz scans (Fig. 5a) show three different components after 14:10 UT: the moving type IV source "M" discussed above, another moving source ("A") and a stationary source ("S"). The source complex was also seen at 237, 327 and 435 MHz (Figs. 5b,c), with about simultaneous start (∼13:37 UT) at all frequencies. Since individual sources cannot be distinguished in the two independent 1D scans before 14:10, the positions of only the brightest source in each 164 MHz scan are plotted in Figs. 4c and d. They scatter above the site where the prominence erupted (Fig. 4c) and where the post-event coronographic image (Fig. 4d) showed a depletion. The height-time plot in Fig. 3 brings order into the complex pattern: sources with different types of radial motion were observed before (∼13:37–13:48 UT; open squares in Figs. 3, 4c), during (∼13:50–13:58 UT; filled triangles) and after (∼13:59–14:11 UT; open diamonds) the passage of the prominence

as extrapolated by the parabolic height-time curve. The 13:50–13:58 UT interval shows emission from the rising prominence or its immediate neighborhood, while the earlier and later emissions came from regions above and below the prominence, respectively.

The stationary type IV source "S" (Fig. 5a) appeared at lower height than the moving sources. It was discernable at 435 MHz since the start of the complex emission at 13:37 UT. In Fig. 4d the radio positions are overlaid on the Hα image showing the flare loops, and on the post-eruptive image of the corona. Contrary to sources A and M source S displayed a clear frequency dispersion of its centroid positions: the higher the frequency, the closer was the source to the solar limb. The stationary radio source lay over the flare loops, but apparently in a large scale structure which in projection extended northward from the site of the flare loops and the filament eruption. The radio sources project to the border of a streamer seen in the Mauna Loa image of Fig. 4d. Radio emission at the NRH and lower frequencies (Tremsdorf Observatory) became invisible around 14:40 UT, while the flare loops continued growing.

2.3. Flaring activity during the eruption

Comparison of the height-time plot in Fig. 3 with radiative signatures shows that the eruption is accompanied by flares. The relative timing resembles the timeline of CME events derived from SMM observations (cf. Harrison et al. 1990, and references therein): a "minor" soft X-ray event occurs at the rise of the mass ejection and is followed by a "major" event after the liftoff. We briefly present the observations and discuss the possibility of a physical link between the flares and the eruptive activity on the limb.

While the prominence started its early rise near 12:56, an impulsive soft X-ray and centimetre wave burst occurred (first grey stripe in Fig. 3) during a flare 70° away in active region NOAA 6257 (∼12:55 UT; *SGD*; cf. Fig. 1a). The centimetre burst was observed at frequencies ≥3 GHz (Bern & Tremsdorf Observatories; courtesy A. Magun, H. Aurass), but no signal was detected at 435 MHz or lower frequencies by the NRH. This implies that electrons were accelerated locally, and remained confined within low-lying structures of AR 6257. There is no evidence for a physical relationship with the prominence eruption besides the time coincidence.

A second flare occurred near 13:26 UT in AR 6263, 57° away from the prominence, during its early accelerated rise and at the start of the surge at the eastern limb (Fig. 3, second grey stripe). The Hα flare (Figs. 4a,b) was accompanied by a group of intense type III bursts from upward travelling electron beams in open magnetic flux tubes. They occurred mainly below 350 MHz (20 to 25 bursts from 13:26:30 to 13:28:50 UT), extending occasionally to ∼450 MHz. The type III emitting electrons were accelerated in the flaring active region, as shown by the source locations during the representative example of Fig. 4a: the projected one-dimensional locations of the source centroids fall in between the Hα flare site and the 164 MHz source. Since the emission at decreasing frequencies comes from regions of ever lower thermal electron density, this points to a a flux tube rooted in AR 6263. A short, diffuse broadband emission (type V continuum, 13:28:45–13:29:05 UT) in the same spectral range as the type III bursts had two sources (Fig. 4b): the north-western one was similar to the type III source, but the projected distance between the sources at different frequencies was greater. This means that the magnetic flux tube had stronger inclination to the line of sight than that of the type III bursts. A second group of sources in the south-eastern quadrant displayed the same ordering as a function of frequency. This geometry is consistent with transequatorial loops connecting AR 6263 and 6267 (cf. Fig. 1a). The loops are about 5×10^5 km long. The source at 164 MHz brightened again for a few seconds at 13:41, i.e. shortly after the start of the continuum around the rising prominence.

Only slowly rising, presumably mainly thermal, microwave emission ("gradual rise and fall") was reported during the type III/V bursts (Tremsdorf Solar Radio Observatory, court. H. Aurass, and *SGD*), indicating that no or few mildly relativistic electrons were injected in the low corona. We note in passing that the soft X-ray time profile steepened during this interval in the same way it does during microwave and hard X-ray emission of impulsive flares (Neupert 1968; Dennis & Zarro 1993). This suggests a close link between the electron acceleration and plasma heating.

The large-scale loop may suggest a connection between the prominence and the remote flare. The flare occurred after the prominence started to rise and cannot be the trigger, contrary to the CMEs studied by Khan & Hudson (2000). The converse is not impossible: a trigger launched in the vicinity of the prominence would have to propagate at ∼800 km s^{-1} along the solar surface or at ∼1200 km s^{-1} along a semi-circular loop. These values are within the range of shock speeds in the corona. But there is no sign of a driver of such a shock, and type II bursts reported by patrol instruments (*SGD* 559-II) started after the flare and type III/V burst.

2.4. Summary of observational results

The Hα and radio imaging observations of the eruptive event on 1990 September 14 showed the following features:

1. A prominence rose with uniformly accelerated motion up to a projected height of ∼0.5 $R_\odot$ above the photosphere. Its uppermost feature was a blob that detached from the body of the prominence in the course of its ascent. Flare loops formed during several hours above the former prominence site.
2. Broadband decimetre-to-metre wave emission started in the vicinity of the detached Hα blob about simultaneously with the appearance of flare loops in the

underlying corona. The source complex displayed various kinds of motion superposed on a general trend of rise similar to the prominence.

3. A moving type IV radio source emerged out of the previous source complex. It was brightest at metre waves, and moved at about constant speed up to $\sim 3\ R_\odot$ above the photosphere. The direction of outward motion changed in the course of the event. This was probably due to successively brightening source components with different time evolution and different circular polarisation.
4. To within the limits of one-dimensional interferometry the centroids of the type IV sources were identical at 164 and 237 MHz, and the source was broader at the lower frequency.
5. While the moving type IV source rose through the corona, a stationary source developed at lower height above a system of flare loops in Hα. These structures were seen on one side of a coronal streamer. The duration of the stationary and moving type IV bursts were comparable at 164 MHz.
6. The various eruptive signatures above the solar limb were accompanied by flares in two active regions on the disk, at heliocentric distances of up to 70° from the prominence. The configuration of radio sources revealed a large-scale magnetic connection between one of these active regions and another one closer to the erupting prominence.

3. Interpretation and discussion

3.1. Structure of the moving radio source

The common centroid position of the moving radio sources at 237 and 164 MHz suggests that a confined electron population, e.g. in a cylindrical volume, was rising as a whole. Since the source was broader at 164 than at 237 MHz, the high-frequency emission appears to come from a shell embedded within the low-frequency source. The observed configuration is clearly different from an expanding loop, where the upward decrease of the magnetic field (gyrosynchrotron emission) or of the thermal electron density (plasma emission) implies that low frequencies are emitted at greater height than high frequencies.

In the following quantitative discussions we approximate the radio emitting structure by a cylindrical volume. But the evolution of polarisation and the trajectory suggest that after ∼14:25 UT a different region of the rising structure radiated at 164 MHz, i.e. that the moving type IV emission comes successively from two different regions within a large rising structure. The different senses of polarisation can be explained by opposite directions of the magnetic field along the line of sight, as expected for a flux rope type geometry, but also by different radiation processes with opposite intrinsic polarisation, e.g. gyrosynchrotron emission and a plasma process. Former work attributed polarisation reversals to the transition from optically thick to thin gyrosynchrotron emission. This would be expected to occur at all frequencies, with a delay at progressively lower frequencies (Dulk 1973). But only the 164 MHz emission reversed polarisation, while the 237 MHz emission faded at that time. Moreover, the low-frequency emission (164 MHz) was brighter than the high-frequency emission (237 MHz). Hence there is no indication for a change from optically thick to thin emission in the observed frequency range. Alternative interpretations exist for the changing trajectory as well. E.g., directional changes of moving type IV bursts were attributed to guiding of the ejecta by the ambient magnetic field (e.g. Dulk et al. 1971; McLean 1973). However, no structure with the appropriate orientation was visible in the pre-event corona (Fig. 1a). The advantage of the picture of two neighbouring radio sources is its ability to explain several features that occur in time coincidence by a common cause.

3.2. Dynamics of the ejecta

The close temporal relationship between the prominence and the moving type IV radio burst is similar to several earlier observations. McLean (1973), Stewart et al. (1978) and Kurokawa et al. (1987), as well as publications reviewed by MacQueen (1980), report events where height-time plots of Hα and radio sources connect continuously to each other, although counter-examples were provided by Riddle (1970) and other work discussed by MacQueen (1980).

The height-time curves of the tip of the prominence (e.g., of the ejected blob) and the centroid of the moving type IV source are to first approximation consistent with the rise of a single magnetic structure seen successively through the Hα emission of the neutral prominence gas and the radio emission of suprathermal electrons. Three different models are used in Fig. 7 to represent the trajectory: uniformly accelerated motion of the prominence and the type IV source (a) and a uniformly accelerated rise of the prominence followed by motion of the type IV source at constant speed (b) or with zero mechanical energy once the gravitational escape speed is attained (ballistic flight; c). The deceleration expected in case (c) is incompatible with the observations, which demonstrates that continuous upward acceleration is required up to a height $\sim 3\ R_\odot$ above the photosphere. Decreasing acceleration is of course expected for a magnetically driven eruption in the corona, and was seen in some observations with Yohkoh-SXT (Klimchuk et al. 1994), LASCO/SoHO (Sheeley et al. 1999; Srivastava et al. 1999; Wood et al. 1999, Fig. 10) and in the combination of Hα and white-light observations (Vršnak 2001). While Fig. 7b is consistent with this expectation, comparison with Fig. 7a illustrates the difficulty to distinguish between trajectories at constant speed and at constant acceleration in the height range 0.5 to 3 $R_\odot$.

The amount of acceleration measured for the prominence lies in the range of values reported by Vršnak (2001)

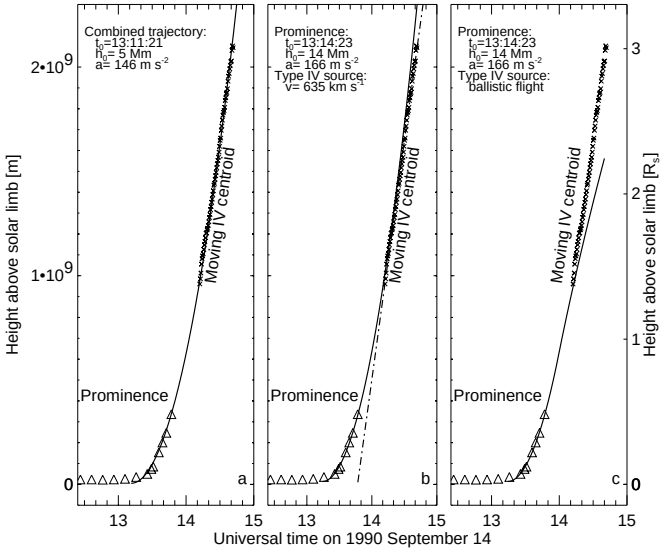

Fig. 7. Height-time plot of the prominence tip in Hα and the centroid of the moving type IV radio source at 164 MHz, compared with different least-squares fits of the trajectory: **a)** quadratic weighted least squares fit to the prominence and moving type IV source; **b)** independent quadratic fit to the prominence (solid line) and linear fit to the type IV source (dashed-dotted); **c)** quadratic fit to the prominence as in **b)** followed by a ballistic flight after the time when the kinetic and potential energy are equal. Only the prominence measurements after 13:10 UT were included in the quadratic fits. Equal weight has been attributed in the fit to the measurements of the prominence and radio positions in **a)**. t_0 is the prominence liftoff time inferred from the quadratic fits, h_0 the height at t_0.

for erupting prominences and inferred from combined Mauna Loa and SMM observations of CMEs at heights $\geq$0.5 $R_\odot$ (St. Cyr et al. 1999), as well as from individual LASCO and EIT analyses (Zhang et al. 2001). The majority of those CMEs had trajectories which were better fit by constant acceleration than by constant speed, and the measured values of acceleration ranged from -200 to $+3000$ m s^{-2}. The strongest accelerations were measured in CMEs associated with active regions. LASCO observations at heights >1 $R_\odot$ (St. Cyr et al. 2000) show a different picture: only 17% of the height-time plots are better fit by constant acceleration than by constant speed, and the accelerations lay within the range (1.4–49) m s^{-2}. Like the 1990 September 14 event most moving type IV bursts are consistent with constant speed at altitudes $\geq$1 $R_\odot$ (Riddle 1970; Sheridan 1977; McLean 1973; Kurokawa et al. 1987), although changes of the intrinsic source structure introduce some uncertainty. Hence the bulk of the Hα, white-light and radio observations suggests that magnetised ejecta are continuously accelerated, but that the acceleration decreases with height.

3.3. Estimate of the mass and energetics of the ejected plasma blob from a radio model

Provided the moving type IV burst arises through plasma emission, we can estimate the mass and mechanical energy of the ejected plasma. For gyrosynchrotron emission the identical sense of polarisation at 164 and 237 MHz implies optically thin emission. For a simple homogeneous source (Dulk & Marsh 1982) the observed brightness temperatures then require a very flat spectrum of mildly relativistic electrons, e.g. a power law with index 1.5 ± 0.7. This appears unrealistic (but the model may be oversimplified). Plasma emission explains easily the different source sizes at 164 and 237 MHz by a thermal electron density that decreases from the axis to the border of the confining volume. Because of the moderate circular polarisation we assume in the following that the observing frequency is twice the local electron plasma frequency (harmonic emission). Sources at 237 and 164 MHz hence outline electron densities of, respectively, 1.7×10^8 and 8.3×10^7 cm^{-3}. We represent these sources by two concentric shells and assume a Gaussian density profile. The diameters of the radio sources measured by the NRH north-south array (1.8×10^5 km at 237 MHz, 2.6×10^5 km at 164 MHz) provide measurements of the widths of the Gaussian at two density levels, from which the central electron density (3.4×10^8 cm^{-3}) and the width at half maximum of the Gaussian (1.8×10^5 km) are inferred. Assuming arbitrarily that the cylinder has a length of 2×10^5 km (the size of the 164 MHz source measured with the east-west array) we calculate the mass of the confined electron-proton plasma. The resulting values for the ejected material, computed from measurements between 14:18 and 14:24 UT, are listed in Table 1. The kinetic energy was evaluated assuming constant mass and using the constant speed of the moving type IV source (Fig. 7b). The potential energy is the energy required to lift this mass from the initial height of the prominence (1.4×10^4 km) to the final height of the moving type IV source at 164 MHz (2.1×10^6 km).

Table 1. Estimated parameters of the ejected plasma blob.

Central electron density	3×10^8 cm^{-3}
Mass	4×10^{15} g
Kinetic energy	9×10^{30} erg
Potential energy	8×10^{30} erg

The major uncertainty of the mass estimate comes from the radiation process. All quantities in Table 1 are upper limits if the radio emission is gyrosynchrotron emission. They must be multiplied by 4 if it is fundamental plasma emission. The incomplete observation of the source geometry adds to the uncertainty.

The estimated mass is within the range of prominence masses derived from SMM coronagraph observations (Illing & Athay 1986). For the largest prominence of this sample, Athay & Illing (1986) estimated a potential energy of 2×10^{31} ergs. Hence the parameters derived from the plasma emission model of the prominence/type IV burst of 1990 September 14 are comparable to Hα analyses of large erupting prominences. They are also comparable to values reported for CMEs by the coronagraphs aboard

Skylab (Rust et al. 1980), Solwind (Webb et al. 1996), SMM (Hundhausen et al. 1994) and SoHO (Lyons et al. 1999; Vourlidas et al. 2000), but are an order of magnitude above estimates from X-ray analyses (Hudson et al. 1996; Gopalswamy et al. 1997). The kinetic energy is near the upper limits of CME values.

3.4. Electron acceleration during the eruptive event

Radio signatures appeared in the vicinity of the prominence only when it was at heights $\geq$0.5 $R_\odot$, without centimetre wave signatures of electrons from the low corona. The radio observations are in qualitative agreement with reconnection in a current sheet below the ejected structure: the moving type IV emission can be understood as being produced by accelerated electrons that get trapped on closed magnetic field lines, while the complex continuum around the rising structure might come from electrons injected onto surrounding open field lines (cf. Scholer et al. 1984, for observations in the magnetotail of the Earth). Simultaneously, electrons accelerated in the current sheet will be injected into sunward retracting reconnected field lines, and may be further accelerated through betatron and Fermi processes. Hot thermal populations will emit soft X-rays in the dense lower-lying loops, while suprathermal electrons produce the stationary type IV burst at greater altitude. The appearance of the stationary type IV source below the rising magnetic structure and above the Hα flare loops agrees with this.

Earlier traces of electron acceleration were observed in remote active regions while the prominence was rising through the corona. It is not clear if there is a physical relationship between these manifestations of activity, but there is no evidence for a triggering of one by the other. The eruption and flares appear as manifestations of localised energy conversion within a large-scale instability that implies multipolar magnetic structures (cf. Delannée & Aulanier 1999; Aulanier et al. 2000).

4. Conclusions

Favourable observing conditions on 1990 September 14 allowed us to track an ejected magnetic structure and electron acceleration in its vicinity as well as in a remote active region at Hα and radio wavelengths. Judging from coronagraphic images taken ~20 hours before and a few hours after the event, the observed activity was related with a coronal mass ejection. The observation and analysis are summarised as follows:

1. The ejected structure showed up as an erupting prominence at heights $\leq$0.5 $R_\odot$ above the limb, and later as a dm-m-wave moving type IV burst at greater altitude. The moving features in the two spectral ranges could be represented by a common trajectory. Continuous acceleration of the ejected structure is required up to about 3 $R_\odot$ above the limb. Both constant acceleration throughout this height range and a decreased acceleration which just compensates for gravitational deceleration at heights $\geq$1 $R_\odot$ are compatible with the data. A ballistic flight at heights (0.5–3) $R_\odot$ is excluded by the measurements.
2. Under the hypothesis that the moving type IV burst is harmonic plasma emission, the mass carried by the ejected magnetic structure can be computed. The inferred value of 4×10^{15} g is comparable to the mass of CMEs and large eruptive prominences. The associated kinetic and potential energies ($\sim 10^{31}$ erg) are near the upper limits of values reported in the literature.
3. Electron acceleration leading to the emission of decimetric and metric radio waves was localised both in the vicinity of the rising structure and in an active region about 60° away. The acceleration near the rising structure is tentatively localised in the current sheet which presumably formed underneath. The acceleration of electron beams in the remote active region is clearly a distinct process, but a physical connection with the prominence eruption may be suggested by the close temporal associations and by the existence of transequatorial loops.

Acknowledgements. The authors benefitted from the generous supply of data by the Solar Data Analysis Center at NASA/GSFC (GOES), High Altitude Observatory (Mauna Loa coronagraph; J. Burkepile & A. Lecinski), Bern University (Microwave whole Sun observations; A. Magun) and from the radio spectrographs in Tremsdorf (H. Aurass) and Nançay (M. Poquérusse). D. Baumont and I. Bualé are thanked for help with the data reduction, A. Klassen for advice on the figures, and F. Chiuderi-Drago for critical reading of the manuscript. The Nançay Radio Observatory is funded by the French Ministry of Education, the CNRS and the Région Centre.

References

Athay, R. G., & Illing, R. M. E. 1986, JGR, 91, 10961
Aulanier, G., DeLuca, E. E., Antiochos, S. K., McMullen, R. A., & Golub, L. 2000, ApJ, 540, 1126
Czaykowska, A., de Ponthieu, B., Alexander, D., & Rank, G. 1999, ApJ, 521, L75
Delannée, C., & Aulanier, G. 1999, Sol. Phys., 190, 107
Demarcq, J., Olivieri, G., Fruteau de Laclos, M., et al. 1985, L'Astronomie, 99, 557
Dennis, B. R., & Zarro, D. M. 1993, Sol. Phys., 146, 177
Démoulin, P., & Vial, J. C. 1992, Sol. Phys., 141, 289
Dulk, G. A. 1973, Sol. Phys., 32, 491
Dulk, G. A., & Marsh, K. A. 1982, ApJ, 259, 350
Dulk, G. A., Stewart, R., Black, H., & Johns, I. 1971, Australian J. Phys., 24, 239
Duncan, R. A. 1981, Sol. Phys., 73, 191
Gopalswamy, N., Hanaoka, Y., Kundu, M. R., et al. 1997, ApJ, 475, 348
Gopalswamy, N., & Kundu, M. R. 1989, Sol. Phys., 122, 91
Hanaoka, Y., Kurokawa, H., Enome, S., et al. 1994, PASJ, 46, 205
Harrison, R. A., Hildner, E., Hundhausen, A. J., Sime, D. G., & Simnett, G. M. 1990, JGR, 95, 917
House, L. L., & Berger, M. A. 1987, ApJ, 323, 406
Hudson, H. S., Acton, L. W., & Freeland, S. L. 1996, ApJ, 470, 629

Hundhausen, A., Stanger, A., & Serbicki, S. 1994, in Solar Dynamic Phenomena and Solar Wind Consequences, ESA SP No. 373, 409–412
Illing, R. M. E., & Athay, G. 1986, Sol. Phys., 105, 173
Khan, J. I., & Hudson, H. S. 2000, GRL, 27, 1083
Khan, J. I., Uchida, Y., McAllister, A. H., et al. 1998, A&A, 336, 753
Klimchuk, J., Acton, L., Harvey, K., et al. 1994, in X-ray solar physics from Yohkoh, ed. Y. Uchida, T. Watanabe, K. Shibata, & H. Hudson (Universal Academy Press Tokyo), 181
Kurokawa, H., Hanaoka, Y., Shibata, K., & Uchida, Y. 1987, Sol. Phys., 108, 251
Lyons, M., Stockton-Chalk, A., & Lewis, D. 1999, in Magnetic Fields and Solar Processes, ESA SP No. 448, 943
MacQueen, R. M. 1980, Royal Society of London Philosophical Transactions Series, 297, 605
McAllister, A., Uchida, Y., Tsuneta, S., et al. 1992, PASJ, 44, L205
McLean, D. J. 1973, PASA, 2, 222
Mouradian, Z., Martres, M. J., Soru-Escaut, I., & Gesztelyi, L. 1987, A&A, 183, 129
Mouradian, Z., Soru-Escaut, I., Hiei, E., et al. 1998, Sol. Phys., 180, 313
Mouradian, Z., Soru-Escaut, I., & Pojoga, S. 1995, Sol. Phys., 158, 269
Mouradian, Z., & Zlicaric, G. 1998, Cartes synoptiques de l'activité solaire, Publ. Observatoire de Paris
Neupert, W. M. 1968, ApJ, 153, L59
Plunkett, S. P., Vourlidas, A., Šimberová, S., et al. 2000, Sol. Phys., 194, 371
Radioheliograph Group. 1989, Sol. Phys., 120, 193
Riddle, A. C. 1970, Sol. Phys., 13, 448
Robinson, R. D. 1978, Sol. Phys., 60, 383
Rompolt, B. 1990, in Hvar Obs. Bull., vol. 14(1), 37
Rust, D. M., Hildner, E., Hansen, R. T., et al. 1980, in Skylab Solar Workshop II, ed. P. Sturrock (Colorado Assoc. Univ. Press), 273
Scholer, M., Klecker, B., Hovestadt, D., et al. 1984, JGR, 89, 6717
Sheeley, N. R., Walters, J. H., Wang, Y., & Howard, R. A. 1999, JGR, 104, 24739
Sheridan, K. V. 1977, PASA, 1, 376
Srivastava, N., Schwenn, R., & Stenborg, G. 1999, in 8th SoHO Workshop, Plasma Dynamics and Diagnostics in the Solar Transition Region and Corona, ESA-SP No. 446, 621
St. Cyr, O. C., Burkepile, J. T., Hundhausen, A. J., & Lecinski, A. R. 1999, JGR, 104, 12493
St. Cyr, O. C., Howard, R. A., Sheeley, N. R., et al. 2000, JGR, 105, 18169
Stewart, R. T. 1985, in Solar Radiophysics: Studies of Emission from the Sun at Metre Wavelengths, ed. D. McLean, & N. Labrum (Cambridge University Press), 361
Stewart, R. T., Dulk, G. A., Sheridan, K. V., et al. 1982, A&A, 116, 217
Stewart, R. T., Hansen, R. T., & Sheridan, K. 1978, in IAU Coll. 44, The Physics of Solar Prominences, ed. E. Jensen, & P. Maltby (Inst. Theoret. Astrophys. Publ., Oslo), 315
Trottet, G., Kerdraon, A., Benz, A. O., & Treumann, R. 1981, A&A, 93, 129
van Driel-Gesztelyi, L., Wiik, J. E., Schmieder, B., et al. 1997, Sol. Phys., 174, 151
Vourlidas, A., Subramanian, P., Dere, K. P., & Howard, R. A. 2000, ApJ, 534, 456
Vršnak, B. 2001, JGR, 106, 25249
Vršnak, B., Ruždjak, V., Rompolt, B., Roša, D., & Zlobec, P. 1993, Sol. Phys., 146, 147
Webb, D. F., Howard, R. A., & Jackson, B. V. 1996, in Solar Wind 8, ed. D. Winterhalter, J. Gosling, S. Habbal, W. Kurth, & M. Neugebauer, AIP Conf. Proc., 382, 540
Wood, B. E., Karovska, M., Chen, J., et al. 1999, ApJ, 512, 484
Zhang, J., Dere, K. P., Howard, R. A., Kundu, M. R., & White, S. M. 2001, ApJ, 559, 452